JM RAPIDS

Stability of a dispersion of elongated particles embedded in a viscous membrane

Harishankar Manikantan†

Department of Chemical Engineering, University of California, Davis, CA 95616, USA

We develop a mean-field model to examine the stability of a 'quasi-2-D suspension' of elongated particles embedded within a viscous membrane. This geometry represents several biological and synthetic settings, and we reveal mechanisms by which the anisotropic mobility of particles interacts with long-ranged viscous membrane hydrodynamics. We first show that a system of slender rod-like particles driven by a constant force is unstable to perturbations in concentration – much like sedimentation in analogous 3-D suspensions – so long as membrane viscous stresses dominate. However, increasing the contribution of viscous stresses from the surrounding 3-D fluid(s) suppresses such an instability. We then tie this result to the hydrodynamic disturbances generated by each particle in the plane of the membrane and show that enhancing subphase viscous contributions generates extensional fields that orient neighbouring particles in a manner that draws them apart. The balance of flux of particles aggregating versus separating then leads to a wave number selection in the mean-field model.

Key words: collective behaviour, suspensions, membranes

1. Introduction

Lipid molecules that comprise the cell membrane are free to flow within the 2-D surface that represents the bilayer, but exchange momentum with the adjacent 3-D medium. Insoluble surfactant monolayers and self-assembled polymer or nanoparticle layers have similar flow physics, driven by this unique 'quasi-2-D' nature of momentum transport. In their seminal work, Saffman & Delbrück ([1975](#)) approximated the membrane as a thin Newtonian fluid layer sandwiched between and coupled to Stokes flow in adjacent 3-D fluid phases. Proteins, ion channels, molecular motors or synthetic particles are embedded in and constrained to move within this 2-D layer. Such a description reveals a subtle

† Email address for correspondence: hmanikantan@ucdavis.edu

transition from 2-D to 3-D hydrodynamics: the interface decouples from the bulk fluid in the 'membrane-dominant' limit when surface viscous stresses far exceed the traction from the surrounding 3-D fluid. This limit is described by the 2-D Stokes equation and has no solution for the steady translation of a cylinder: a consequence of the Stokes paradox (Manikantan & Squires 2020). However, Saffman (1976) recognized that subphase viscous stresses eventually catch up with surface viscous stresses beyond a critical length scale, ultimately regularizing the divergence inherent to 2-D Stokes flow. Building on this framework, the hydrodynamics of disks (Hughes, Pailthorpe & White 1981; Stone & Ajdari 1998), spheres (Danov, Dimova & Pouligny 2000; Fischer, Dhar & Heinig 2006), rods (Fischer 2004; Levine, Liverpool & MacKintosh 2004) and ellipsoids (Stone & Masoud 2015) embedded in surface viscous interfaces are now firmly established, and widely employed in quantifying lateral diffusion in membranes, monolayers and biofilms.

Most of these efforts, however, address flow around single particles. Correlated diffusion and collective effects become relevant in biological membranes that contain a high concentration of proteins (Bussell, Koch & Hammer 1995; Oppenheimer & Diamant 2009). Recent efforts have highlighted the role of long-ranged hydrodynamics in aggregating and assembling active (Oppenheimer, Stein & Shelley 2019; Manikantan 2020) and driven (Vig & Manikantan 2023) membrane-bound point particles. While a point-particle description offers useful insight into this complex problem, real particles have a finite size and orientability with anisotropic hydrodynamic mobilities (Fischer 2004; Levine *et al.* 2004) that lead to non-trivial dynamics (Camley & Brown 2013; Shi, Moradi & Nazockdast 2022). Cellular processes such as signalling, trafficking and curvature sensing are associated with the transport and reorganization of filamentous proteins and rod-like domains (Simunovic, Srivastava & Voth 2013) on the plasma membrane. Recent advances also enable synthetic assembly of catalytic (Dhar *et al.* 2006) and DNA origami-based (Khmelinskaia *et al.* 2021) nanorods embedded in monolayers and membranes, yet no description of their collective surface viscous interactions yet exist.

We aim to address this gap by borrowing fluid mechanical insights from analogous works on the dynamics of 3-D suspensions of settling particles. Such a 3-D problem was first studied by Koch & Shaqfeh (1989) who showed that a dispersion of settling spheroids is inherently unstable to concentration fluctuations. Elongated particles realign parallel to the extensional axis of the hydrodynamic disturbance generated by its neighbours. The orientation of each particle then dictates the direction and speed of settling due to the anisotropy in its hydrodynamic mobility. Disturbance fields due to denser particle clusters reorient neighbouring particles in such a way that they preferentially migrate towards regions of already dense clusters, thereby amplifying concentration fluctuations. Using a linear stability analysis, Koch & Shaqfeh (1989) showed that fluctuations with the longest wavelengths are the most unstable in a homogeneous 3-D suspension of isotropically oriented spheroids. In what follows, we will adapt such a mathematical framework to examine orientation-dependent hydrodynamic interactions and microstructure within a viscous membrane.

In § 2 we develop a mean-field description of a dilute quasi-2-D suspension of driven membrane-attached slender particles by coupling their anisotropic mobilities to long-ranged interfacial viscous hydrodynamics. In § 3, we analyse the linear stability of such a system to concentration perturbations, revealing signatures of the resolution of the Stokes paradox in collective dynamics. In § 4, we connect straining fields set up around driven particles to suspension stability and reveal mechanisms for a length-scale selection in this problem.
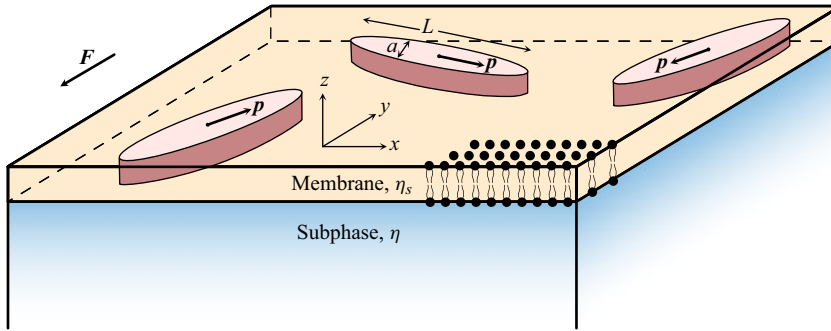
Figure 1. System geometry: elongated particles ($L \gg a$) are embedded within an infinitesimally thin 2-D viscous layer atop a 3-D fluid subphase, and are all driven in the membrane plane by an external force $\boldsymbol{F}$.

2. Theoretical formulation

2.1. *Mean-field description*

The geometry of our system is shown in figure 1. Slender rod-like particles of length L and characteristic thickness a (with $a \ll L$), each with a unit orientation vector $\boldsymbol{p} = (\cos\theta, \sin\theta)$, are embedded within a 2-D viscous layer atop a 3-D subphase. In a mean-field description, we define a probability distribution $\psi(\boldsymbol{x}, \boldsymbol{p}, t)$ such that the local concentration $c(\boldsymbol{x}, t)$ is obtained by integrating ψ across all possible orientations $\boldsymbol{p}$:

$$c(\boldsymbol{x}, t) = \int \psi(\boldsymbol{x}, \boldsymbol{p}, t)\, \mathrm{d}\boldsymbol{p} = \int_0^{2\pi} \psi(\boldsymbol{x}, \boldsymbol{p}, t)\, \mathrm{d}\theta. \tag{2.1}$$

We will also define n as the number density of particles:

$$n = \frac{1}{A} \int_A c(\boldsymbol{x}, t)\, \mathrm{d}\boldsymbol{x}, \tag{2.2}$$

where A is the area of the membrane. Rods are constrained to translate and rotate in the plane of the membrane. Conservation of particles is then expressed by

$$\frac{\partial \psi}{\partial t} + \boldsymbol{\nabla}_s \cdot (\dot{\boldsymbol{x}}\psi) + \boldsymbol{\nabla}_p \cdot (\dot{\boldsymbol{p}}\psi) = 0, \tag{2.3}$$

where $\dot{\boldsymbol{x}}$ and $\dot{\boldsymbol{p}}$ are translational and rotational velocities that capture probability flux. The surface gradient operator in the plane of the membrane is defined as $\boldsymbol{\nabla}_s = (\boldsymbol{I} - \boldsymbol{nn}) \cdot \boldsymbol{\nabla}$, where $\boldsymbol{I}$ is the identity tensor and $\boldsymbol{n}$ is the local normal to the 2-D manifold that represents the membrane, and the orientational gradient operator simplifies to

$$\boldsymbol{\nabla}_p = (\boldsymbol{I} - \boldsymbol{pp}) \cdot \frac{\partial}{\partial \boldsymbol{p}} = \hat{\boldsymbol{\theta}} \frac{\partial}{\partial \theta}. \tag{2.4}$$

Here, $\hat{\boldsymbol{\theta}}$ is the azimuthal unit vector in the plane of the membrane. In this initial work, we will restrict ourselves to planar membranes at $z = 0$, and so $\boldsymbol{n} = \hat{\boldsymbol{z}}$, where $\hat{\boldsymbol{z}}$ is the unit vector in the z direction (figure 1).

2.2. *Micromechanical model*

We will explore the response of such a quasi-2-D suspension of elongated particles to an externally applied force. For simplicity, the force $\boldsymbol{F}$ will be taken to be a constant and act

in the same direction on all particles, akin to sedimentation in 3-D suspensions (Koch & Shaqfeh 1989). This might represent tethered trans-membrane proteins that are driven by the external environment or by the cytoskeleton; alternatively, this geometry represents proteins or probes dragged through a membrane or a monolayer by an external force. The translational velocity in (2.3) then has contributions from the self-mobility of each particle, and from advection due to the disturbance field generated by neighbouring rods:

$$\dot{\boldsymbol{x}} = \boldsymbol{u}_s + \boldsymbol{u}_d. \tag{2.5}$$

Phospholipids that make up biological membranes and monolayers are insoluble and well-approximated as 2-D incompressible fluids (Manikantan & Squires 2020). The disturbance field $\boldsymbol{u}_d$ then solves the Boussinesq–Scriven equation (Scriven 1960) for the stress balance within a viscous incompressible interface of surface viscosity η_s coupled to 3-D Stokes flow in the adjacent bulk fluid of viscosity η and forced by $\boldsymbol{F}$ distributed at concentration $c(\boldsymbol{x}, t)$:

$$\boldsymbol{\nabla}_s \Pi = \eta_s \nabla_s^2 \boldsymbol{u}_d - \eta \left. \frac{\partial \boldsymbol{v}}{\partial z} \right|_{z=0} + \boldsymbol{F} c(\boldsymbol{x}, t), \quad \boldsymbol{\nabla}_s \cdot \boldsymbol{u}_d = 0. \tag{2.6a,b}$$

Here, Π is the surface pressure. Membrane flow is coupled to the 3-D flow field $\boldsymbol{v}$ in the adjacent semi-infinite (z from 0 to $-\infty$) subphase via the traction term and a no-slip condition $\boldsymbol{u} = \boldsymbol{v}$ at $z = 0$. This framework can be generalized to accommodate membrane curvature and to the presence of 3-D fluids on either side of the membrane (Shi *et al.* 2022; Shi, Moradi & Nazockdast 2024).

The velocity $\boldsymbol{u}_s$ in (2.5) is the local response of a rod-like particle to a constant force $\boldsymbol{F}$:

$$\boldsymbol{u}_s = \mu_\perp (\boldsymbol{I} - \boldsymbol{pp}) \cdot \boldsymbol{F} + \mu_\parallel \boldsymbol{pp} \cdot \boldsymbol{F}, \tag{2.7}$$

with hydrodynamic mobilities $\mu_\perp$ and $\mu_\parallel$ for translation in directions perpendicular and parallel to $\boldsymbol{p}$, respectively. These mobilities can be determined by adapting standard boundary integral methods to a slender rod. In short, this is achieved by evaluating the disturbance velocity due to a line distribution of point-force solutions of the Boussinesq–Scriven equation (2.6a,b), and then integrating the force density that satisfies the boundary condition corresponding to particle motion parallel or perpendicular to the force (Fischer 2004; Levine *et al.* 2004; Shi *et al.* 2022). These integrals can be analytically performed in the asymptotic limits of membrane-dominant ($\eta_s \gg \eta L$) or subphase-dominate ($\eta_s \ll \eta L$) systems. Specifically, the hydrodynamic mobilities of a rod in a planar incompressible membrane when surface viscous stresses dominate ($\eta_s/(\eta L) \to \infty$) are (Fischer 2004)

$$\mu_\parallel = \frac{\log(8\eta_s/(\eta L)) - \gamma_E + 1/2}{4\pi\eta_s}, \quad \mu_\perp = \frac{\log(8\eta_s/(\eta L)) - \gamma_E - 1/2}{4\pi\eta_s}, \tag{2.8a,b}$$

where γ_E is Euler's constant. Notably, drag on a rod-like particle depends only weakly on its length and orientation unlike in 3-D fluids where $\mu_\parallel^{3D} \approx 2\mu_\perp^{3D}$. However, the parallel and perpendicular mobilities are not identical ($\mu_\parallel - \mu_\perp \to 1/(4\pi\eta_s)$ as $\eta_s/(\eta L) \to \infty$) and the resulting anisotropy, although weak, affects the suspension microstructure as we see in §§ 3–4. By contrast, the mobilities for subphase-dominant systems ($\eta_s/(\eta L) \to 0$) limit to

$$\mu_\parallel = \frac{\ln(0.48\eta L/\eta_s)}{\pi\eta L}, \quad \mu_\perp = \frac{1}{\pi\eta L}. \tag{2.9a,b}$$

Perpendicular translation in a nearly inviscid membrane represents the most striking difference with 3-D fluids: in-plane 2-D incompressibility displaces surface velocities (and

therefore bulk streamlines) around the length of the rod giving rise to a perpendicular drag that is linear in L. Mobility coefficients $\mu_\parallel$ and $\mu_\perp$ for intermediate values of $\eta_s/(\eta L)$ can be evaluated numerically (Fischer 2004; Levine *et al.* 2004) and they monotonically interpolate between (2.8*a,b*) and (2.9*a,b*); further, $\mu_\parallel$ is always greater than $\mu_\perp$.

Finally, the rotational flux in (2.3) captures reorientation due to non-uniform disturbance fields. For slender rod-like particles, this is given by Jeffery's equation (Jeffery 1922):

$$\dot{\boldsymbol{p}} = (\boldsymbol{I} - \boldsymbol{pp}) \cdot \nabla_s \boldsymbol{u}_d \cdot \boldsymbol{p}. \tag{2.10}$$

Thermal noise may contribute additional terms to $\dot{\boldsymbol{x}}$ and $\dot{\boldsymbol{p}}$, or equivalently as diffusive terms in the conservation equation (2.3). We ignore diffusion in what follows to highlight the role of hydrodynamics alone. However, diffusion is straightforward to add to the analysis below via an additional flux $-D\nabla_s(\ln \psi)$ or equivalently directly as a diffusive term $D\nabla_s^2 \psi$ on the right-hand side of (2.3), where D is a diffusion constant. Diffusion always acts to suppress large wavenumber fluctuations (Manikantan *et al.* 2014; Vig & Manikantan 2023).

3. Linear stability

We wish to examine the linear stability of a dilute quasi-2-D suspension that is homogeneous in concentration and isotropic in orientational distribution. The disturbance field associated with such a base state is $\boldsymbol{u}_d = \boldsymbol{0}$. We perturb the probability distribution around this base state as $\psi(\boldsymbol{x}, \boldsymbol{p}, t) = n[\psi_0 + \epsilon \psi'(\boldsymbol{x}, \boldsymbol{p}, t)]$ where $\psi_0 = (2\pi)^{-1}$, $\boldsymbol{u}_d = \epsilon \boldsymbol{u}_d'$ and $\dot{\boldsymbol{p}}_d = \epsilon \dot{\boldsymbol{p}}_d'$. Here, $|\epsilon| << 1$ and primes represent perturbed quantities. The corresponding local concentration is $c = n[1 + \epsilon c']$. Plugging perturbed quantities into (2.3) and recognizing the isotropic base state as well as 2-D incompressibility of the membrane fluid field ($\nabla_s \cdot \boldsymbol{u} = 0$) gives the probability conservation equation at $O(\epsilon)$:

$$\frac{\partial \psi'}{\partial t} + \nabla_s \psi' \cdot \boldsymbol{u}_s + \psi_0 \nabla_p \cdot \dot{\boldsymbol{p}}_d' = 0 \tag{3.1}$$

We then impose normal modes with wave vector $\boldsymbol{k}$ and frequency ω of the form

$$\psi'(\boldsymbol{x}, \boldsymbol{p}, t) = \tilde{\psi}(\boldsymbol{k}, \boldsymbol{p}, \omega) \exp(\mathrm{i}(\boldsymbol{k} \cdot \boldsymbol{x} - \omega t)), \tag{3.2}$$

where tildes represent corresponding Fourier variables, so that $\tilde{c}(\boldsymbol{k}, \omega) = \int \tilde{\psi} \, \mathrm{d}\boldsymbol{p}$ is the associated local concentration. The associated hydrodynamic disturbance field can be obtained by solving (2.6*a,b*) for the corresponding Fourier transform of the disturbance velocity (Manikantan & Squires 2020):

$$\tilde{\boldsymbol{u}}_d(\boldsymbol{k}, \boldsymbol{p}, \omega) = \frac{(\boldsymbol{I} - \hat{\boldsymbol{k}}\hat{\boldsymbol{k}}) \cdot nF\tilde{c}}{k^2 \eta_s + k\eta}, \tag{3.3}$$

where $k = |\boldsymbol{k}|$ and $\hat{\boldsymbol{k}} = \boldsymbol{k}/k$ is a unit vector. Then, using Jeffery's equation (2.10), we find

$$\tilde{\dot{\boldsymbol{p}}}_d = \frac{\mathrm{i}(\boldsymbol{p} \cdot \boldsymbol{k})(\boldsymbol{I} - \boldsymbol{pp}) \cdot (\boldsymbol{I} - \hat{\boldsymbol{k}}\hat{\boldsymbol{k}}) \cdot nF\tilde{c}}{k^2 \eta_s + k\eta} \Rightarrow \nabla_p \cdot \tilde{\dot{\boldsymbol{p}}}_d = \frac{-2\mathrm{i}(\boldsymbol{p} \cdot \boldsymbol{k})\boldsymbol{p} \cdot (\boldsymbol{I} - \hat{\boldsymbol{k}}\hat{\boldsymbol{k}}) \cdot nF\tilde{c}}{k^2 \eta_s + k\eta}. \tag{3.4}$$

Plugging (3.2) and (3.4) into (3.1) gives

$$(-\mathrm{i}\omega + \mathrm{i}\boldsymbol{k} \cdot \boldsymbol{u}_s)\tilde{\psi} - \frac{2\mathrm{i}\psi_0(\boldsymbol{p} \cdot \boldsymbol{k})\boldsymbol{p} \cdot (\boldsymbol{I} - \hat{\boldsymbol{k}}\hat{\boldsymbol{k}}) \cdot nF\tilde{c}}{k^2 \eta_s + k\eta} = 0, \tag{3.5}$$

where $\boldsymbol{u}_s$ follows (2.7).

We now non-dimensionalize over characteristic values of L for length, F for force, and $F/(4\pi\eta_s)$ for velocities. We will take the direction of the force to be $\hat{f}$ so that $\boldsymbol{F} = F\hat{f}$. Then,

$$(-\omega + \boldsymbol{k} \cdot [\mu_{\parallel}\boldsymbol{pp} + \mu_{\perp}(\boldsymbol{I} - \boldsymbol{pp})] \cdot \hat{f})\tilde{\psi} - \frac{8N\psi_0\ell(\boldsymbol{p} \cdot \boldsymbol{k})\boldsymbol{p} \cdot (\boldsymbol{I} - \hat{k}\hat{k}) \cdot \hat{f}\tilde{c}}{k^2\ell + k} = 0, \quad (3.6)$$

where $\ell = \eta_s/(\eta L)$ is the dimensionless Saffman–Delbrück length. Alternatively, ℓ can be interpreted as a Boussinesq number (Manikantan & Squires 2020) which characterizes surface viscous stresses relative to 3-D viscous stresses from the adjacent subphase fluid over the length L. Momentum transport is membrane-dominated when $\ell \to \infty$ and subphase-dominated when $\ell \to 0$. The variable $N = n\pi L^2$ is an effective area fraction occupied by particles. The long-ranged description is valid only in the dilute regime, and so N is at most $O(1)$.

To proceed, we simplify our problem by considering only perturbations in concentration along the direction perpendicular to the external forces: $\boldsymbol{k} \cdot \hat{f} = 0$. This is motivated by the fact that these transverse perturbations are the most unstable in analogous 3-D sedimentation problems (Koch & Shaqfeh 1989) and driven 2-D suspensions (Vig & Manikantan 2023). Simplifying with this assumption and rearranging gives

$$\tilde{\psi} = \left(\frac{8N\psi_0\ell\tilde{c}}{k^2\ell + k}\right) \frac{(\boldsymbol{p} \cdot \boldsymbol{k})(\boldsymbol{p} \cdot \hat{f})}{(\mu_{\parallel} - \mu_{\perp})(\boldsymbol{p} \cdot \boldsymbol{k})(\boldsymbol{p} \cdot \hat{f}) - \omega}. \quad (3.7)$$

Integrating (3.7) across all orientations while noting that $\tilde{c}(\boldsymbol{k}, \omega) = \int \tilde{\psi} \, \mathrm{d}\boldsymbol{p}$ eliminates $\tilde{\psi}$ to reveal an implicit relationship for $\omega(k)$:

$$\int \frac{(\boldsymbol{p} \cdot \boldsymbol{k})(\boldsymbol{p} \cdot \hat{f})}{(\mu_{\parallel} - \mu_{\perp})(\boldsymbol{p} \cdot \boldsymbol{k})(\boldsymbol{p} \cdot \hat{f}) - \omega} \mathrm{d}\boldsymbol{p} = \frac{k^2\ell + k}{8N\psi_0\ell}. \quad (3.8)$$

The mobility coefficients $\mu_{\parallel}$ and $\mu_{\perp}$ are functions of ℓ, and $\psi_0 = (2\pi)^{-1}$ is the isotropic base state distribution. For a given area fraction N, (3.8) thus represents a family of dispersion relations parametrized by the Saffman–Delbrück length ℓ.

In a 2-D Cartesian plane representing the membrane, we can take $\hat{f} = -\hat{y}$ and $\hat{k} = \hat{x}$ without loss of generality. Simplifying (3.8) using $\boldsymbol{p} = (\cos\theta, \sin\theta)$ then gives

$$\frac{1}{2\pi} \int_0^{2\pi} \frac{k\sin\theta\cos\theta}{(\mu_{\parallel} - \mu_{\perp})k\sin\theta\cos\theta + \omega} \mathrm{d}\theta = \frac{k^2\ell + k}{8N\ell}, \quad (3.9)$$

which is an implicit integral equation for the dispersion relation $k(\omega)$. For normal modes of the form $\exp[\mathrm{i}(\boldsymbol{k} \cdot \boldsymbol{x} - \omega t)]$, perturbations are unstable if the imaginary part of ω is positive.

Figure 2(*a*) shows the growth rate $\sigma = \mathrm{Im}[\omega]$ as a function of wavenumber obtained by numerically evaluating roots of (3.9) with a secant method. The $\ell \to \infty$ limit is reminiscent of analogous 3-D suspensions, where the system-spanning mode corresponding to $k = 0$ is the most unstable (see Koch & Shaqfeh 1989; Manikantan *et al.* 2014). To obtain the growth rate at $k = 0$ analytically, we expand the integrand in (3.9) as
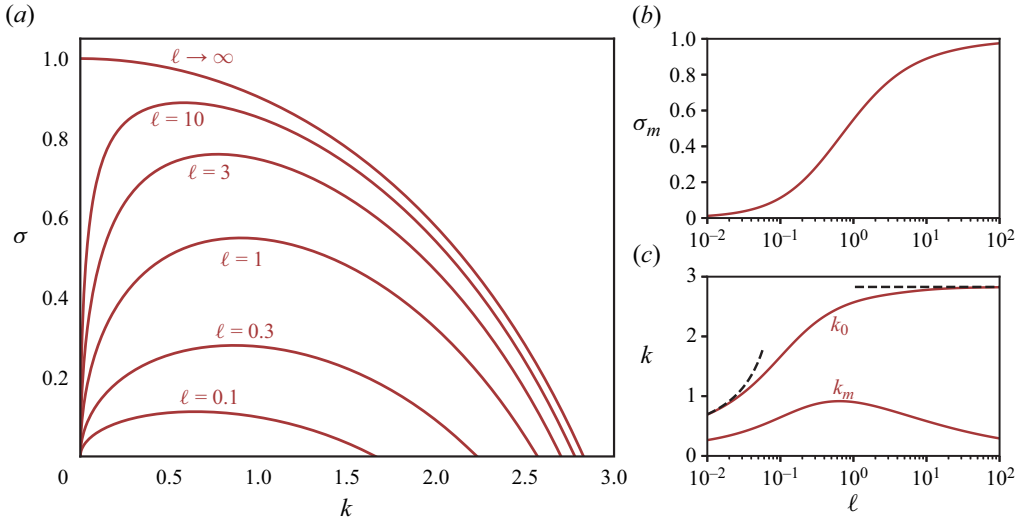
Figure 2. (*a*) Growth rates σ of unstable modes at various $\ell = \eta_s/\eta L$ for a dimensionless number density of $N = n\pi L^2 = 1$. (*b*) Maximum growth rate σ_m, and (*c*) most unstable wavenumber k_m and largest wavenumber k_0 as a function of ℓ. Dashed lines in (*c*) are asymptotic limits from (3.14*a*,*b*).

a Taylor series in k:

$$\frac{k}{2\pi\omega} \int_0^{2\pi} \sin\theta\cos\theta \left[1 - \frac{(\mu_\parallel - \mu_\perp)k}{\omega}\sin\theta\cos\theta + \cdots\right] d\theta = \frac{k^2\ell + k}{8N\ell}. \tag{3.10}$$

Integrating term by term and simplifying gives

$$-\frac{(\mu_\parallel - \mu_\perp)k^2}{\omega^2} + O(k^4) = \frac{k^2\ell + k}{N\ell}. \tag{3.11}$$

From (2.8*a*,*b*), the dimensionless mobility difference in the membrane-dominated regime ($\ell \to \infty$) is $\mu_\parallel - \mu_\perp \to 1$, which gives $\omega^2 = -N + O(k^2)$ or

$$\sigma(k \to 0, \ell \to \infty) = \sqrt{N}. \tag{3.12}$$

In fact, this turns out to be the maximum value of the growth rate across all k and ℓ.

Increasing subphase viscous stresses (decreasing ℓ) always acts to suppress the instability. Notably, the $k = 0$ mode is stable for finite η, reflecting a boundary layer at infinity that regularizes the singularity in 2-D Stokes by accounting for subphase viscous stresses (Saffman 1976). For finite ℓ, (3.11) gives $\omega^2 \sim -kN\ell(\mu_\parallel - \mu_\perp)$ or $\sigma = \text{Im}[\omega] \propto \sqrt{k}$. In other words, the growth rate goes to zero as $k \to 0$ for all values of ℓ except in the limit $\ell \to \infty$. The most unstable mode then corresponds to a finite value of k which suggests a mechanism for wavenumber selection. The most unstable wavenumber k_m can be determined by taking the derivative of (3.9) with respect to k and numerically solving the implicit integral equation corresponding to $\partial\omega/\partial k = 0$. Figure 2(*b*,*c*) shows k_m and the corresponding growth rate σ_m as a function of ℓ. Note that the maximum growth rate σ_m asymptotes to the $\ell \to \infty$ limit as predicted by (3.12), and monotonically decreases upon decreasing ℓ. The wavenumber k_m corresponding to fastest growth of perturbations, however, varies non-monotonically with ℓ and peaks at $\ell = O(1)$: in §4 we propose a mechanism of instability that clarifies the length scale selection underlying k_m and its dependence on ℓ.

Finally, a key parameter is the largest unstable wavenumber k_0 which reveals the length scale of shortest unstable modes. Setting $\omega = 0$ in (3.9) gives

$$k_0^2 \ell + k_0 = \frac{8N\ell}{\mu_\parallel - \mu_\perp}. \tag{3.13}$$

Solving this quadratic equation for positive k_0 yields the curve in figure 2(*c*). Note that this $\omega = 0$ limit is only valid for $k \neq 0$. The range of unstable modes increases monotonically with ℓ. The high and low ℓ limits can be found analytically using (2.8*a,b*) and (2.9*a,b*): $\mu_\parallel - \mu_\perp$ asymptotes to 1 and $4\ell[\ln(0.48/\ell) - 1]$ in these limits, respectively, giving

$$k_0(\ell \to \infty) = \sqrt{8N}, \quad k_0(\ell \to 0) = \frac{2N}{-\log(\ell) - 1.73}. \tag{3.14a,b}$$

These are shown as the dashed curves in figure 2(*c*).

4. Instability mechanism and length-scale selection

The mechanism of instability can be understood by examining the disturbance flow created in the plane of the membrane by a point force and the effect of this flow on realigning neighbouring particles. We again follow classic 3-D suspension works (Koch & Shaqfeh 1989) to examine relative alignment of pairs of particles under a pseudo-steady approximation where particle positions are held at a fixed distance. In a dilute suspension, any given particle creates a point-force velocity disturbance (shown as the arrow pointing downward in figure 3*a,b*). Neighbouring particles tend to align parallel to the direction of the extensional component (shown in magenta around each particle) of the fluid motion caused by the point force at the centre. Such a picture helps identify microstructural configurations that favour accumulation or separation.

We can evaluate the local extensional flow and the principal axes of extension around each particle from the hydrodynamic disturbance field due to the point force. The dimensionless velocity at a point r in the plane of the membrane due to a point force at the origin is (Fischer 2004; Levine *et al.* 2004; Manikantan & Squires 2020)

$$\boldsymbol{u}(\boldsymbol{r}) = \pi \left[\left(\frac{H_1(d)}{d} - \frac{2}{\pi d^2} - \frac{Y_0(d) + Y_2(d)}{2} \right) \frac{\boldsymbol{rr}}{r^2} \right.$$
$$\left. + \left(H_0(d) - \frac{H_1(d)}{d} + \frac{2}{\pi d^2} - \frac{Y_0(d) - Y_2(d)}{2} \right) \left(\boldsymbol{I} - \frac{\boldsymbol{rr}}{r^2} \right) \right] \cdot \hat{\boldsymbol{f}}, \tag{4.1}$$

where $r = |\boldsymbol{r}|$ is the dimensionless distance, and $d = r/\ell$. Here, H_ν and Y_ν are Struve and Bessel functions of the second kind or order ν, respectively. Note that ℓ is renormalized by the distance r in the far-field description: in other words, at constant η_s and η, the system switches from membrane-dominated to subphase-dominated at large enough length scales.

The velocity field in the plane of the membrane from (4.1) asymptotes to that corresponding to the 2-D stokeslet in the membrane-dominated regime ($\ell \gg r$):

$$\boldsymbol{u}(r, \ell \gg r) \to \left[-\log\left(\frac{r}{\ell}\right) \boldsymbol{I} + \frac{\boldsymbol{rr}}{r^2} \right] \cdot \hat{\boldsymbol{f}}. \tag{4.2}$$

The mechanism of the instability is tied to the reorientation of neighbouring particles when placed in such a disturbance field. Specifically, rod-like particles align with the extensional
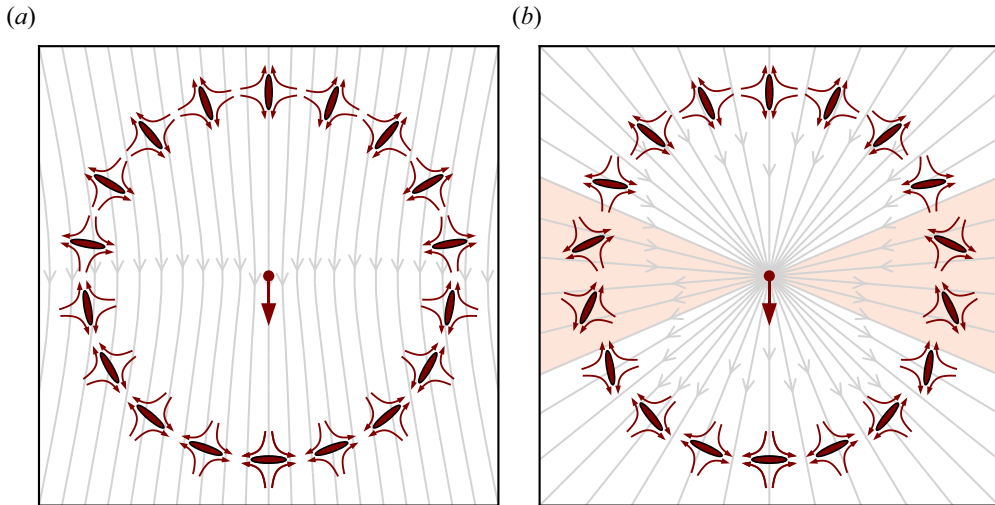
(*a*)   (*b*)

Figure 3. Mechanism of the instability: a point force generates in-plane velocity $\boldsymbol{u}$ (grey streamlines). The magenta streamlines depict the symmetric part of the local, linear flow field around particles at a distance r. Particles are shown in their most favoured orientation, with their long axis parallel to the extensional component of the flow field generated by the point force. (*a*) For $\ell \gg r$ (membrane-dominated regime), neighbours always reorient such that they are drawn towards the point force, thereby increasing particle density. (*b*) By contrast, at much longer length scales $r \gg \ell$ (subphase-dominated regime), particles that fall within the shaded region reorient such that they are drawn away from the point force, reducing particle density and stabilizing the suspension. For a fixed η_s and η, the system transitions continuously from membrane-dominated to subphase-dominated at large enough distances.

axis of the local flow. The rate-of-strain tensor in the membrane-dominated case is

$$\boldsymbol{E}(\ell \gg r) = \frac{\boldsymbol{\nabla}_s \boldsymbol{u}_d + \boldsymbol{\nabla}_s \boldsymbol{u}_d^T}{2} = \frac{(\boldsymbol{r} \cdot \hat{\boldsymbol{f}})\boldsymbol{I}}{r^2} - \frac{2\boldsymbol{r}\boldsymbol{r}\boldsymbol{r} \cdot \hat{\boldsymbol{f}}}{r^4}. \tag{4.3}$$

Using $\hat{\boldsymbol{f}} = -\hat{\boldsymbol{y}}$ and $\boldsymbol{r} = r\hat{\boldsymbol{r}} = (r\cos\phi, r\sin\phi)$ where ϕ is measured relative to the positive x direction diagonalizes the rate-of-strain tensor in the $(\hat{\boldsymbol{r}}, \hat{\boldsymbol{\phi}})$ basis as

$$\boldsymbol{E}(\ell \gg r) = \frac{\sin\phi}{r} \begin{bmatrix} 1 & 0 \\ 0 & -1 \end{bmatrix}. \tag{4.4}$$

The eigenvectors of $\boldsymbol{E}$ are the principal directions of extension. We see from (4.4) that the principal axis of extension is parallel to $\hat{\boldsymbol{r}}$ – i.e. along the line connecting the particle to the point force – in the upper half-plane ($\phi > 0$) and perpendicular to $\hat{\boldsymbol{r}}$ in the lower half ($\phi < 0$). Figure 3(*a*) shows particles in such a preferred alignment: the anisotropic mobility of each elongated particle then draws it towards the point force, leading to a net tendency for particles to accumulate and amplify concentration fluctuations. This is analogous to the classic 3-D instability in the suspension of a rod (see Koch & Shaqfeh 1989). Note also from (4.4) that the eigenvalues of $\boldsymbol{E}(\ell \gg r)$, corresponding to the local rates of extension λ_{ext}, peak at $\phi = \pm\frac{1}{2}\pi$ and vanish at $\phi = 0$: rods on the same horizontal line thus do not reorient in response to the disturbance due to the other.

The in-plane extensional field surrounding a point force changes dramatically upon increasing the contribution from the subphase (decreasing ℓ). The membrane velocity field

in the surface-inviscid limit ($\ell \ll r$) is

$$\boldsymbol{u}(r, \ell \ll r) \to 2\ell \frac{\boldsymbol{rr}}{r^3} \cdot \hat{\boldsymbol{f}}. \tag{4.5}$$

Note that (4.5) is not simply a 2-D slice of the flow due to a point force in the bulk 3-D fluid: surface incompressibility requires that $\boldsymbol{u}$ be divergence-free in the plane of the membrane. The rate-of-strain tensor is no longer easily diagonalizable in the $(\hat{\boldsymbol{r}}, \hat{\boldsymbol{\phi}})$ basis; however, $\boldsymbol{E}$ still reveals key features when expressed in the $(\hat{\boldsymbol{x}}, \hat{\boldsymbol{y}})$ basis:

$$\boldsymbol{E}(\ell \ll r) = \frac{2\ell}{r^2} \begin{bmatrix} \sin\phi(3\cos^2\phi - 1) & \cos\phi\left(3\sin^2\phi - \frac{1}{2}\right) \\ \cos\phi\left(3\sin^2\phi - \frac{1}{2}\right) & \sin\phi(3\sin^2\phi - 2) \end{bmatrix}. \tag{4.6}$$

First, principal rates of extension scale with ℓ, consistent with a weakening instability as seen in § 3. Additionally, neighbouring particles along the wave vector (on the same horizontal line as the point force, or along $\phi = 0$) experience a non-zero rate of extension along a principal direction $\theta_{ext} = 3\pi/4$ (figure 4). Coupled to the anisotropic mobility of rods, local extension therefore reorients rods in a manner that draws them away from the reference particle if initially placed in a region near $\phi = 0$, which acts as a stabilizing mechanism. Note also from (4.6) that $\boldsymbol{E}$ is diagonal in the $(\hat{\boldsymbol{x}}, \hat{\boldsymbol{y}})$ basis when $3\sin^2\phi = \frac{1}{2}$, i.e. for a critical angle $\phi_c = \pm \sin^{-1}(1/\sqrt{6})$. This corresponds to principal axes that are aligned with $\hat{\boldsymbol{x}}$ or $\hat{\boldsymbol{y}}$ and reveals a transition from configurations that draw neighbouring particles towards the point force (when $|\phi| > |\phi_c|$) or away from it. This also suggests a mechanism for wavenumber selection as seen in the stability analysis in § 3: the critical length scale emerges from a balance of fluxes of particles driven out from within the region $|\phi| < |\phi_c|$ vs drawn in from regions where $|\phi| > |\phi_c|$.

Principal directions of extension for arbitrary ℓ, obtained by numerically evaluating the eigenvectors of $\boldsymbol{E}$ from the general velocity field in (4.1), are shown in figure 4(*a*). This further clarifies the emergence of a 'stabilizing region' in terms of preferred orientations for finite ℓ. Particles placed in this region are drawn away from the reference particle, contributing to a suppression of the instability. The $\ell/r \to \infty$ limit avoids this region entirely as seen mechanistically in figure 3 and quantitatively as a discontinuity in $\theta_{ext}(\phi)$ in figure 4(*a*). This reflects the singularity of 2-D Stokes flow at infinity, and the subphase viscous contribution introduces a boundary layer that regularizes this discontinuity. In doing so, θ_{ext} takes on values that fall within the shaded patch in figure 4(*a*) that represents a stabilizing region, where particle orientations are such that they are drawn away from the reference particle. This mechanism also explains the stabilization of the $k = 0$ mode for finite ℓ in § 3: for any η and η_s (and since $\boldsymbol{k}$ is parallel to $\hat{\boldsymbol{x}}$ for transverse perturbations), particles along the horizontal line ($\phi = 0$) will always fall in the stabilizing region at a large enough value of r.

The associated eigenvalues of $\boldsymbol{E}$ are local rates of extension λ_{ext}: while these principal rates always peak at $\phi = \pm\frac{1}{2}\pi$ and their magnitudes decrease upon decreasing ℓ, they do not always vanish at $\phi = 0$ (figure 4*b*,*c*). Indeed, $\lambda_{ext}(r, \phi = 0)$ peaks when $r \sim \ell$. For a pair of particles placed in the same horizontal line, the reorientation that favours particle separation is thus strongest at distances comparable to the Saffman–Delbrück length.

5. Conclusion

In this paper, we developed a mean-field model to examine hydrodynamic collective modes of elongated particles embedded in viscous membranes or monolayers. We focused on a
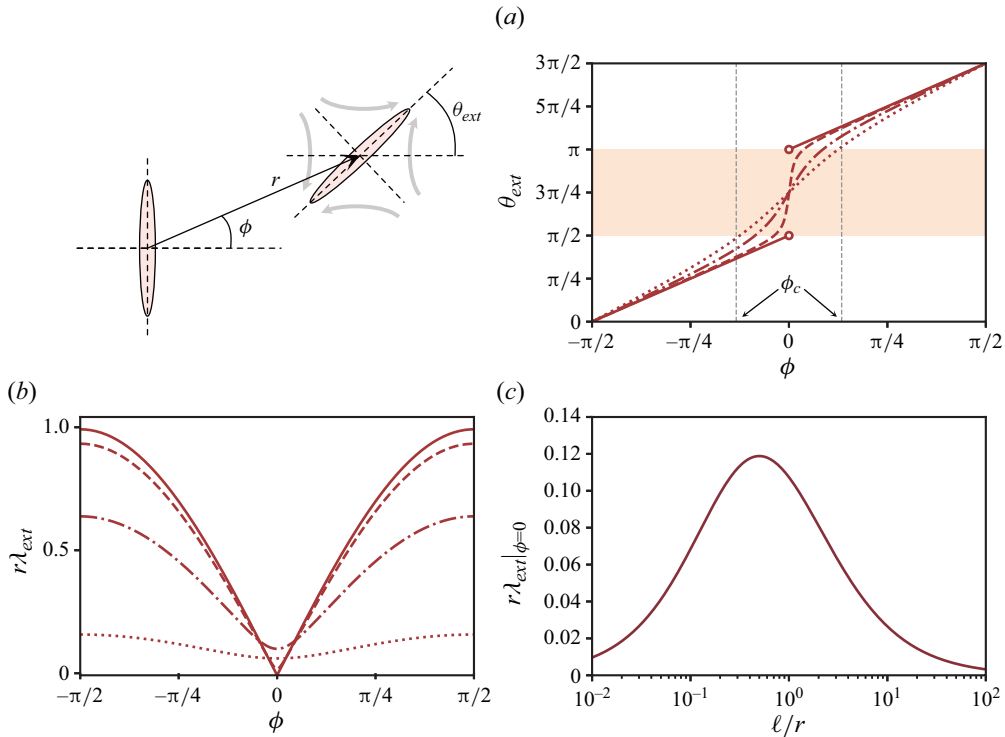
(a)

Figure 4. (a) Principal axes of stretch θ_{ext} corresponding to preferred orientation of a neighbouring particle as a function of azimuthal position ϕ around a reference particle for $\ell/r = 0.1$ (dotted line), 1 (dash-dot) and 10 (dashed line). The shaded patch denotes the set of orientations that draws particles away from each other: this region is not accessed in the limit of $\ell \to \infty$ (solid line), whereas $\ell \to 0$ maximizes this window for a range of relative positions $|\phi| < |\phi_c| = \sin^{-1}(1/\sqrt{6})$. (b) Principal rates of extension λ_{ext} corresponding to cases shown in (b). (c) The principal rate λ_{ext} does not vanish at $\phi = 0$ for finite ℓ, and peaks when $r \sim \ell$.

linear stability analysis around a homogeneous and isotropic quasi-2-D suspension of such particles. We discover a unique mechanism for stabilization of such a system, reflecting aspects of the Stokes paradox in 2-D viscous flows and its regularization via 3-D subphase stresses. We then tie this mechanism to the interplay between anisotropic particle mobility and long-ranged hydrodynamics in the plane of the membrane.

More generally, this mean-field framework opens a rich avenue of fluid dynamical problems and tools to examine microstructure on biological or synthetic membranes. The method can be readily adapted to membranes with curvature using modified Green's functions (Shi *et al.* 2022, 2024), to active particles on membranes via a stresslet solution (Oppenheimer *et al.* 2019; Manikantan 2020), and to systems with weakly non-Newtonian membrane rheology using tools such as the Lorentz reciprocal theorem (Vig & Manikantan 2023). We have illustrated the 'deep' subphase limit: confining the 3-D fluid has been shown to amplify bulk stresses (Camley & Brown 2013; Shi *et al.* 2024) and modify membrane flow fields in manners that favour aggregation (Manikantan 2020). This modification is also straightforward within the mean-field description developed here. Our findings also open up opportunities to examine nonlinear dynamics in these systems by computationally solving the mean-field model and through efficient particle simulations of crowded systems. Building on these insights, we anticipate that the present work will spur new directions of fluid dynamical studies into active and passive quasi-2-D suspensions.

Author ORCIDs.

Ⓓ Harishankar Manikantan https://orcid.org/0000-0002-4270-3527.

REFERENCES

BUSSELL, S.J., KOCH, D.L. & HAMMER, D.A. 1995 Effect of hydrodynamic interactions on the diffusion of integral membrane proteins: diffusion in plasma membranes. *Biophys. J.* **68** (5), 1836–1849.

CAMLEY, B.A. & BROWN, F.L.H. 2013 Diffusion of complex objects embedded in free and supported lipid bilayer membranes: role of shape anisotropy and leaflet structure. *Soft Matt.* **9** (19), 4767.

DANOV, K.D., DIMOVA, R. & POULIGNY, B. 2000 Viscous drag of a solid sphere straddling a spherical or flat surface. *Phys. Fluids* **12** (11), 2711–2722.

DHAR, P., FISCHER, T.M., WANG, Y., MALLOUK, T.E., PAXTON, W.F. & SEN, A. 2006 Autonomously moving nanorods at a viscous interface. *Nano Lett.* **6** (1), 66–72.

FISCHER, T.M. 2004 The drag on needles moving in a Langmuir monolayer. *J. Fluid Mech.* **498**, 123–137.

FISCHER, T.M., DHAR, P. & HEINIG, P. 2006 The viscous drag of spheres and filaments moving in membranes or monolayers. *J. Fluid Mech.* **558**, 451–475.

HUGHES, B.D., PAILTHORPE, B.A. & WHITE, L.R. 1981 The translational and rotational drag on a cylinder moving in a membrane. *J. Fluid Mech.* **110**, 349–372.

JEFFERY, G.B. 1922 The motion of ellipsoidal particles immersed in a viscous fluid. *Proc. R. Soc. Lond.* A **102** (715), 161–179.

KHMELINSKAIA, A., FRANQUELIM, H.G., YAADAV, R., PETROV, E.P. & SCHWILLE, P. 2021 Membrane-mediated self-organization of rod-like DNA origami on supported lipid bilayers. *Adv. Mater. Interfaces* **8**, 2101094.

KOCH, D.L. & SHAQFEH, E.S.G. 1989 The instability of a dispersion of sedimenting spheroids. *J. Fluid Mech.* **209**, 521–542.

LEVINE, A.J., LIVERPOOL, T. & MACKINTOSH, F. 2004 Dynamics of rigid and flexible extended bodies in viscous films and membranes. *Phys. Rev. Lett.* **93** (3), 038102.

MANIKANTAN, H. 2020 Tunable collective dynamics of active inclusions in viscous membranes. *Phys. Rev. Lett.* **125** (26), 268101.

MANIKANTAN, H., LI, L., SPAGNOLIE, S.E. & SAINTILLAN, D. 2014 The instability of a sedimenting suspension of weakly flexible fibres. *J. Fluid Mech.* **756**, 935–964.

MANIKANTAN, H. & SQUIRES, T.M. 2020 Surfactant dynamics: hidden variables controlling fluid flows. *J. Fluid Mech.* **892**, P1.

OPPENHEIMER, N. & DIAMANT, H. 2009 Correlated diffusion of membrane proteins and their effect on membrane viscosity. *Biophys. J.* **96** (8), 3041–3049.

OPPENHEIMER, N., STEIN, D.B. & SHELLEY, M.J. 2019 Rotating membrane inclusions crystallize through hydrodynamic and steric interactions. *Phys. Rev. Lett.* **123** (14), 148101.

SAFFMAN, P.G. 1976 Brownian motion in thin sheets of viscous fluid. *J. Fluid Mech.* **73**, 593–602.

SAFFMAN, P.G. & DELBRÜCK, M. 1975 Brownian motion in biological membranes. *Proc. Natl Acad. Sci. USA* **72** (8), 3111–3113.

SCRIVEN, L.E. 1960 Dynamics of a fluid interface: equation of motion for Newtonian surface fluids. *Chem. Engng Sci.* **12** (2), 98–108.

SHI, W., MORADI, M. & NAZOCKDAST, E. 2022 Hydrodynamics of a single filament moving in a spherical membrane. *Phys. Rev. Fluids* **7** (8), 1–16.

SHI, W., MORADI, M. & NAZOCKDAST, E. 2024 The drag of a filament moving in a supported spherical bilayer. *J. Fluid Mech.* **979**, A6.

SIMUNOVIC, M., SRIVASTAVA, A. & VOTH, G.A. 2013 Linear aggregation of proteins on the membrane as a prelude to membrane remodeling. *Proc. Natl Acad. Sci. USA* **110** (51), 20396–20401.

STONE, H.A. & AJDARI, A. 1998 Hydrodynamics of particles embedded in a flat surfactant layer overlying a subphase of finite depth. *J. Fluid Mech.* **369** (1), 151–173.

STONE, H.A. & MASOUD, H. 2015 Mobility of membrane-trapped particles. *J. Fluid Mech.* **781**, 494–505.

VIG, V. & MANIKANTAN, H. 2023 Hydrodynamic aggregation of membrane inclusions due to non-Newtonian surface rheology. *Phys. Fluids* **35** (6), 1–13.